Depolarization of light in turbid media: a scattering event resolved Monte Carlo study

Xinxin Guo,[3,*] Michael F. G. Wood,[1] Nirmalya Ghosh,[4] and I. Alex Vitkin[1,2]

[1]Division of Biophysics and Bioimaging, Ontario Cancer Institute and Departments of Medical Biophysics, University of Toronto, 610 University Avenue, Toronto, ON M5G 2M9, Canada

[2]Radiation Oncology, University of Toronto, 610 University Avenue, Toronto, ON M5G 2M9, Canada

[3]Department of Mechanical and Industrial Engineering, University of Toronto, 5 King's College Road, Toronto, ON M5S 3G8, Canada

[4]IISER Kolkata, Mohanpur Campus, PO: BCKV Campus Main Office, Mohanpur-741252, West Bengal, India

*Corresponding author: guox@mie.utoronto.ca

Received 8 July 2009; revised 23 November 2009; accepted 24 November 2009; posted 30 November 2009 (Doc. ID 114000); published 7 January 2010

Details of light depolarization in turbid media were investigated using polarization-sensitive Monte Carlo simulations. The surviving linear and circular polarization fractions of photons undergoing a particular number of scattering events were studied for different optical properties of the turbid media. It was found that the threshold number of photon scattering interactions that fully randomize the incident polarization (defined here as $<1\%$ surviving polarization fraction) is not a constant, but varies with the photon detection angle. Larger detection angles, close to backscattering direction, show lower full depolarization threshold number for a given set of sample's optical properties. The Monte Carlo simulations also confirm that depolarization is not only controlled by the number of scattering events and detection geometry, but is also strongly influenced by other factors such as anisotropy g, medium linear birefringence, and the polarization state of the incident light.

OCIS codes: 260.5430, 170.7050, 290.4210.

1. Introduction

The pursuit to understand the mechanisms of light depolarization in multiply-scattering media began decades ago, and the search continues with renewed enthusiasm [1–8]. The growing interest is partly due to the potential applications of the polarized light in biomedical diagnostics. One example is the application to blood glucose sensing [9–11], where the optical rotation of the incident light and/or the glucose-induced refractive index matching effect may be related to tissue/blood glucose concentration. However, photons propagating in a multiply scattering media, such as biological tissue, lose their polarization information as a result of scattering. This makes the polarization-state-tracking techniques difficult and even impossible as the light becomes fully depolarized. Thus it is of significant importance to properly understand the mechanisms of polarization randomization in turbid media. Many prior studies have tackled this problem through analytical methods and simulations or through experimental methods to predict and evaluate the depolarization behavior. However, those methods yield largely qualitative and macroscale results, not precise enough to quantify when and how the polarization information is lost (e.g., the number of scattering events before $<1\%$ degree of polarization remains, defined here as the full depolarization threshold). Recently, Monte Carlo simulations have been used to study the light scattering in turbid media in terms of scattering

0003-6935/10/020153-10$15.00/0

orders [1,12–17]. Detailed descriptions of forward- or side-scattered light [12–14,16] through low turbidity samples and backscattered light from high turbidity samples [1,15,17] were obtained, and the effects of the scattering properties and detection geometries on the light were examined. However, in all the above investigations, the turbid samples were limited to slab (cube) or semi-infinite geometry.

In this paper, we present a quantitative and microscale (scattering-event resolved) study of depolarization of light propagating through a cylindrical turbid sample, a geometry that may be useful in the context of blood glucose sensing due to its curvature similarity to finger tips and lips, using a polarization-sensitive Monte Carlo (MC) model developed in our group [18–20]. Since backward detection may have distinctive advantages in a clinical setting and in enhanced photon polarization preservation, our study focused on the depolarization of light scattered into the backward hemisphere. Specifically, we considered the cylindrical geometry and examined the effects of detection geometry, optical properties of the turbid media, and the state of initial polarization on the depolarization.

In the MC simulations, the detected photons were tracked by the number of scattering events they underwent, and polarization properties of each photon group were examined as a function of this number. This "zoom-in" method allows us to examine the depolarization evolution with the scattering events in detail, and pinpoint the full depolarization threshold. This depolarization study, combined with our previous photon path length distribution research [6], may provide useful insights for polarimetric applications, especially for those using polarization-gating techniques. For example, as shown in greater detail in Subsection 3.A, we demonstrate that for a given number of scattering events, a larger portion of polarization-maintaining photons may be obtained at a detection angle smaller than the exact backscattering direction. Thus the imaging using the polarization-gating method may have better contrast at a detection angle off the exact backscattering direction. Another potentially useful insight we discuss in Subsection 3.B is that unlike overall collected photons, for a certain number of scattering events, the depolarization of the photon subpopulation collected at a given angle may decrease with the increase of the turbidity of the media. Therefore, precaution should be taken in the diagnosis of a lesion in tissue by relating photon depolarization to the lesion-induced change in the tissue scattering coefficient. To ensure accurate and realistic predictions, our MC model of polarized light propagation in a complex turbid medium includes the effects of linear birefringence caused by anisotropic tissue structures (e.g., collagen and muscle). This is particularly important for biomedical polarimetry, as many biological tissues at accessible anatomical sites (e.g., skin) exhibit birefringent properties.

2. Theory

A. Monte Carlo Simulations

In our polarization-sensitive and validated Monte Carlo simulation [18–20], based on the previous models of Kaplan *et al.* [21] and Jaillon *et al.* [22], the photons are propagated between scattering events within a turbid sample. The Stokes 1×4 vector, describing light polarization states [$S = (I \quad Q \quad U \quad V)^T$, where I is light intensity, Q and U are horizontal and vertical linear polarization, and V is circular polarization] is transformed by the application of the 4×4 Mueller matrix describing the effects of an optical element on the light polarization state. The current study modeled the turbid medium as consisting of monodispersed polystyrene microsphere scatterers suspended in water, whose Mueller matrix could be calculated analytically from Mie theory [23]. Other polarization-modifying effects of the medium, such as linear birefringence due to structural anisotropy and circular birefringence due to chiral (optically active) molecules, were modeled via the modified N-matrix formalism as the photons propagated between the scattering events [20].

Explicitly, the position, propagation direction, and polarization of a photon are initialized at the entrance of a cylindrical sample 40 mm in height and 8 mm in diameter. The cylindrical interface is characterized by 144 surface elements: 48 rectangular elements forming the sides and 48 triangular elements forming the top and the bottom faces. Since the side element is narrow ($\sim$0.5 mm), its curvature can be ignored, so each rectangular side element is treated as a plane (0.52 mm $\times$ 40 mm). The photon propagates between scattering events within the sample if it does not cross the interface. The Stokes vector of the photon is transformed by the application of the Mueller matrix of the microsphere-caused scattering event, which is calculated from Mie theory [23]. When birefringence is present, specified by the extraordinary axis with refractive index n_e and the ordinary axis with refractive index n_o, the refractive index difference results in the retardation of orthogonal linear polarization states. The birefringence effect is thus modeled through the application of the Mueller matrix for a retarder, applied to the Stokes vectors of the photon between the scattering events. As mentioned, the Monte Carlo model can simulate the effects of both linear and circular birefringence (in addition to multiple scattering), via the N-matrix formulation suitable for handling simultaneous effects described by noncommuting matrices [20].

If the photon encounters the sample boundary, its Stokes vector is transformed into the Fresnel reference frame. The internal and external refractive indices are set to 1.33 (for water) and 1 (for air). The photon's Stokes vector and propagation direction are modified based on whether the photon is reflected or transmitted. The probability of transmission or reflection is calculated from the polarization-dependent Fresnel coefficients and the polarization state of the

photon at that point. If the photon is reflected, the propagation inside the sample continues. If the photon is transmitted, the macroscopic values of the Stokes coefficients are obtained from the sum of the Stokes vector components of emerging photons.

The transmitted photons are binned spatially into the surface elements, which are further divided vertically into smaller surface detection elements (0.52 mm × 0.98 mm). The photons can also be binned angularly within each surface detection element based on the exit angle that the propagation vector of the photon makes with the normal to the interface. Figure 1 is the schematic diagram of the cylindrical sample. A polarized beam enters the sample at O at the center of the vertically oriented cylinder. The escaping photons exit the sample at point $P(\theta, \psi)$ on the cylinder within a solid angle 2δ. δ is the angle that the propagation vector of the emerging photons makes with the normal to the interface, defined as acceptance angle (from 0° to 90°). θ is the angle between the forward direction and the normal of the surface detection element, defined as the detection angle [from 0° (forward) to 180° (backward)]. ψ is defined as azimuthal angle (from −90° to 90°), at which the photons exit the sample relative to the horizontal (x–y) plane. **b** is the orientation of the extraordinary axis when linear birefringence is considered. Unless specified otherwise, we chose the size of the surface detection elements to be ∼0.5 mm^2, the acceptance angle $\delta = 48°$, and $\psi = 0$ to simulate our experimental system [24]. Note that the size of the surface detection element and the value of the acceptance angle δ both affect the detected degree of photon polarization. The extent of the effects varies with detection geometry; we briefly revisit this issue in Subsection 3.A.

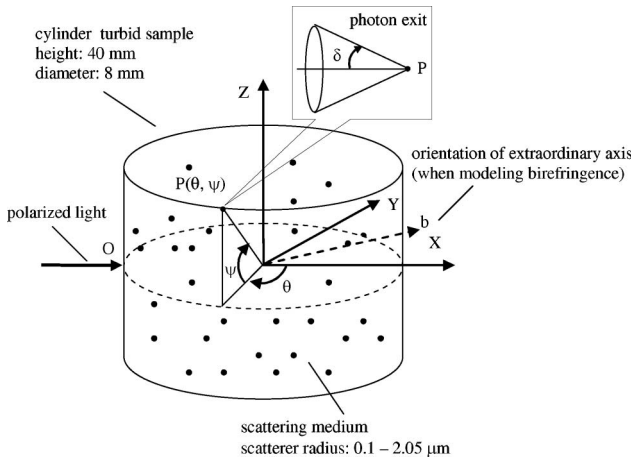

Fig. 1. Cylindrical geometry used in the MC simulations. Linearly (in x–y plane) or circularly polarized light incidents at O on a vertically oriented cylindrical sample, 40 mm in height and 8 mm in diameter. The turbid sample is modeled as a water suspension with polystyrene spherical scatterers (0.1 to 2.05 μm in radius). The scattered light is collected by a small detector element at $P(\theta, \psi)$ on the surface of the cylinder with an acceptance angle δ. θ is the detection direction (the angle between the forward direction X and the normal to the detector element); ψ is the azimuthal angle at P. When modeling birefringence, an extraordinary axis **b** oriented in the x–y (incident) plane is assumed.

The detected photons are tabulated based on the number of scattering events they undergo within the sample, which is the key investigation method employed in this study.

B. Monte Carlo Simulation Input and Output

A large number (10^9) of horizontally or circularly polarized photons with a wavelength of 632.8 nm were launched in the simulations. The initial Stokes vectors were $S_i = (1 \quad 1 \quad 0 \quad 0)^T$ for horizontally linear polarization input (in x–y plane of Fig. 1), and $S_i = (1 \quad 0 \quad 0 \quad 1)^T$ for circular polarization input. The beam size was 1 mm in diameter.

The output photons from the simulations were binned based on the number of scattering events, N, experienced within the sample. The bin number, N, varied from 1 up to ∼70, beyond which there was no remaining polarization recorded. There was also a N-unresolved cumulative bin, referred to as Total, containing all the collected photons without discrimination (that is, N varied from 1 to some large unbounded number). The parameters obtained from the simulations were thus indexed (β_{LN}, β_{CN}, DOP_N, and I_N) and cumulative (β_{LT}, β_{CT}, DOP_T, N_a, and I_T). β_{LN} and β_{CN} are the surviving linear and circular polarization fractions of the photons in bin N, DOP_N is the overall degree of polarization after N scatterings ($=\beta_{LN} + \beta_{CN}$), I_N is the number of photons (polarized and depolarized) in bin N. β_{LT}, β_{CT}, and I_T are the corresponding parameters for the bin Total, DOP_T is the total degree of polarization of the photons (with $\mathrm{DOP}_T = \beta_{LT} + \beta_{CT}$), and N_a is the average number of scattering events of the total collected photons, defined as

$$N_a = \frac{\sum_{N=1}^{\infty} N I_N}{I_T}. \tag{1}$$

C. Optical Properties of the Turbid Media

The turbid sample was modeled as a suspension of monodispersed polystyrene microspheres in water. The refractive indices of the scattering particles and medium were n_m 1.59 and $n_o = 1.33$, respectively. When the birefringence effect was studied, an extraordinary refractive index $n_e = 1.3301$ in value and 45° in the x–y plane direction was implemented (i.e., $n_e - n_o = 0.0001$), which is fairly typical of biological tissue [25]. The scattering coefficient of the medium μ_s ranged from 50 to 300 cm^{-1}. For most simulations, μ_s was set to 100 cm^{-1} to approximate the typical turbidity of biological tissue. The absorption coefficient was set to 0.00326 cm^{-1} for water at incident wavelength $\lambda = 632.8$ nm. A range of scatterer sizes (radius r, from 0.1 to 2.05 μm) was used to generate different scattering anisotropy g (equal to the cosine of the average scattering angle), resulting in g values from 0.32 to 0.93 [23]. This microspheres-in-water formulation also allowed the calculation of the medium scattering Mueller matrix to be used in the Monte Carlo simulations (see Subsection 2.A).

3. Results and Discussion

A. Depolarization by Scattering

To study the depolarization by scattering, linearly polarized photons were launched into a turbid medium with scattering coefficient $\mu_s = 100\,\mathrm{cm}^{-1}$ (scatterer radius $r = 2.05\,\mu\mathrm{m}$, $g = 0.89$). The scattered photons were collected in the incident x–y plane ($\psi = 0°$), at detection angle θ from 99° to 180°. Figure 2 displays three typical variations of the surviving linear polarization fraction β_{LN} as a function of the number of scattering events N, obtained at detection angle $\theta = 99°$, 135°, and 180°. As expected, all three curves show a decreasing trend with increasing N. But the three curves start at a different number of scattering events $N:1$ for $\theta = 180°$, 17 for $\theta = 135°$, and 40 for $\theta = 99°$. In turbid media, the mechanism for photon redirection is the scattering process. Because of the geometry of O (entrance) relative to P (exit), single scattering is enough for photons to be backscattered ($\theta = 180°$) out of the sample, whereas at least ~17 and ~40 scattering events are needed for the photons to exit at $\theta =$ 135° and 99°, respectively. So only the photons undergoing at least ~17 scatterings can be observed at $\theta = 135°$, and photons undergoing at least ~40 scatterings can be observed at $\theta = 99°$. It is also noticed from Fig. 2 that the same number of scattering events can yield different depolarization. For example, for $N = 40$, β_{LN} at $\theta = 180°$ and 135° has dropped to 4% and 17%, respectively, but it remains as high as 50% at $\theta = 99°$ This indicates that the depolarization depends not only on the number of the scattering events, but also on the redirection that scattering has caused and thus the detection direction. For this turbid medium with anisotropy $g = 0.89$, which favors forward scattering, 40 scattering events cause

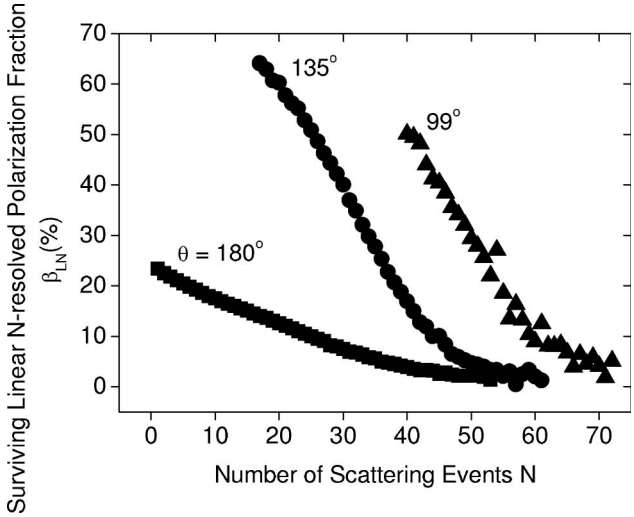

Fig. 2. Scattering dependence of depolarization. Surviving linear polarization fraction β_{LN} versus the number of scattering events N (from 1 to 72). The photons were collected at detection angles $\theta =$ 180° (solid square), 135° (solid circle) and 99° (solid triangle) at fixed azimuthal angle $\psi = 0°$ and acceptance angle $\delta = 48°$.

greater depolarization for the photons exiting from $\theta = 180°$ than the photons exiting from $\theta = 99°$. Examining the N that causes >99% depolarization (defined here as the full depolarization threshold), we note that it is also not unique but also depends on the detection angle θ. The full (linear) depolarization appears at $N \sim 50$ for $\theta = 180°$, $N \sim 60$ for $\theta = 135°$, and $N \sim 70$ at 99°. Thus, fewer scattering events are more effective in depolarizing the light as one approaches the backscattering direction.

An additional interesting result from Fig. 2 warrants further discussion. The surprisingly low linear polarization fraction for $\theta = 180°$ with $N = 1$ (single backscattering) might be due to the finite size of the detection elements and beam size, and symmetric polarization patterns of singly backscattered light [21]. Theoretically, single scattering does not depolarize the light, thus we expect β_L to remain close to ~100% after $N = 1$; however, the finite detection element size causes singly backscattered light with opposite linear polarization to be scored, resulting in a reduction in overall linear polarization. Additional simulations showed an increase in β_L with decreasing detection element size and acceptance angle δ after single scattering, in support of this explanation. For example, at the same acceptance angle $\delta(48°)$, β_L increased to 35% when the detection element was decreased from 0.5 to $0.3\,\mathrm{mm}^2$. Further, for the same $0.5\,\mathrm{mm}^2$ detection element size, β_L increased to 27% as the acceptance angle was reduced to 20°. It is shown in Subsection 3.B that the nonunity value of the surviving polarization fraction of the single-scattered light is scatterer-size dependent (and scattering-anisotropy dependent) as well. In fact, the nonunity degree of polarization in a backward single-scattering regime was also observed by other groups [26–28]. Jiao *et al.* [26] and Lee *et al.* [27] reported <100% degree of polarization in intralipid solutions for both linearly polarized and circularly polarized light using the polarization-sensitive OCT technique, with the degree of polarization also being intralipid concentration dependent. Sakami and Dogariu [28] reported <100% degree of polarization in absorbing and scattering medium for both linearly and circularly polarized incident light using a time-revolved discrete-ordinates method, with the resultant degree of polarization being influenced by the source–detector geometry.

B. Depolarization Dependence on Optical Properties of Turbid Media

Changes in optical properties of the turbid media, such as scattering coefficient μ_s, anisotropy g, and birefringence, also influence light depolarization statistics to a significant extent.

Figure 3(a) shows the scattering coefficient (μ_s) dependence of surviving linear polarization fraction (β_{LN}) for photons encountering a particular number of scattering events ($N = 1$ and 45) before escaping from the turbid medium. The results are shown for three different detection angles ($\theta = 180°$, 135°,

and 121°). These N values were specially chosen for the selected geometries—for $\theta = 180°$, $N = 1$ is of particular interest; for $\theta = 135°$ and 121°, $N = 45$ yields meaningful β_{LN} values. As seen, for $N = 1$ and for detection angle $\theta = 180°$, β_{LN} is not sensitive to a change in the value for μ_s, with the value remaining almost constant at ~22% for the range of μ_s from 50 to 250 cm^{-1}. Since the singly backscattered photons leave the media after they encounter the first scatterer, the value for μ_s only influences, on an average, how far the photons travel within the media before that scattering event occurs. Therefore in this case, the degree of polarization of the photons should not be influenced by a change in the value for μ_s, as confirmed by the displayed results.

Significantly different trends are seen for the other ($\theta = 135°$ and 121°) detection geometries. Somewhat counterintuitively, the surviving linear polarization fraction is observed to increase with an increasing value for μ_s for these detection directions. In a turbid medium, depolarization of linearly polarized light primarily arises due to the randomization of the electric field vector's direction resulting from a random sequence of scattering events at arbitrary angles. Since large-angle scattering events lead to stronger randomization of the field vector's direction, photons experiencing a series of large-angle scattering events are depolarized to a larger extent than those experiencing small angle scattering events (even though the number of scattering events N may be the same). It may happen for a subpopulation of photons, encountering a certain number of scattering events ($N = 45$ here) and escaping the medium through a certain direction ($\theta = 135°$ and 121° here), the trajectories are such that, on average, the photons experience more large-angle scattering events for a lower value of μ_s. Note that for a fixed value of N and θ, the average photon path length is also larger for lower μ_s (because the scattering mean free path is larger for lower μ_s). Thus the angular randomization of the field vector's direction for this subpopulation of photons is stronger for a lower value of μ_s, leading to stronger depolarization. However, when summed over all the scattering events, the total surviving linear polarization fraction (β_{LT}) should decrease with an increasing scattering coefficient. This follows because, for lower μ_s, the overall distribution shifts to a smaller number of scattering events (a significantly larger contribution of subpopulation of photons with lower N), leading to weaker net depolarization (when summed over all N) for lower μ_s. This indeed is the case, as can be seen from Fig. 3(b), where β_{LT} decreases gradually with increasing μ_s for the three examined detection angles.

Results from the MC study also show that the variation in anisotropy g of the turbid media influences the light depolarization, as illustrated in Fig. 4. Different anisotropies were achieved by changing the scatterer size (radius) in the simulations, while the scattering coefficient μ_s was kept constant at 100 cm^{-1}. Figure 4(a) shows the relationship between

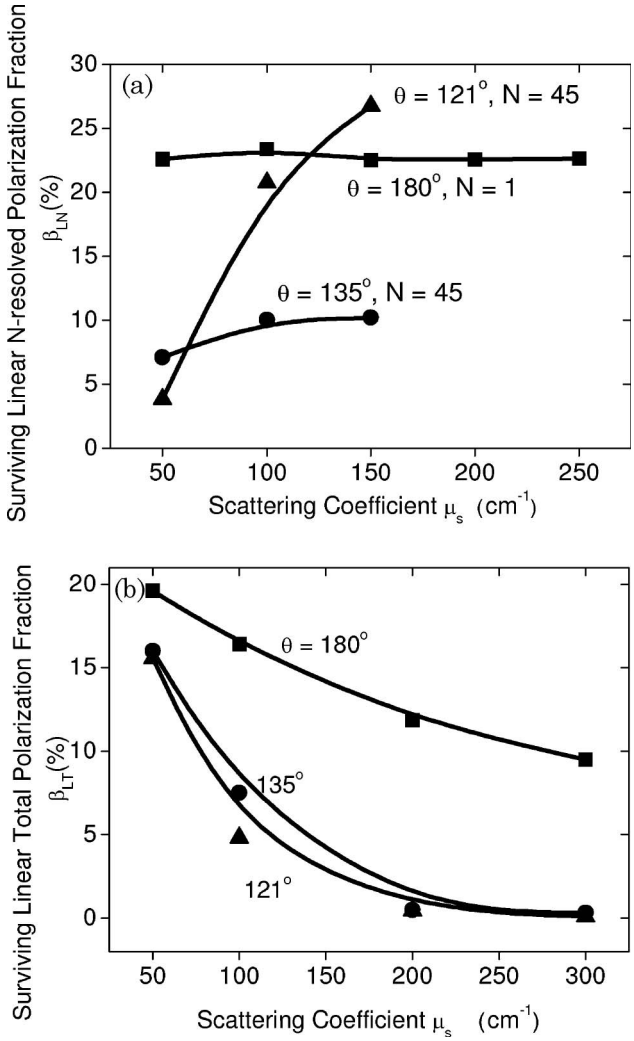

Fig. 3. Scattering coefficient effect on depolarization. (a) surviving linear polarization fraction β_{LN} versus scattering coefficient μ_s (from 50 to 250 cm^{-1}) at different detection angles θ and the number of scattering events N: square + line is for $\theta = 180°$, $N = 1$; circle + line is for $\theta = 135°$, $N = 45$; triangle + line is for $\theta = 121°$, $N = 45$. (b) Total surviving linear polarization fraction β_{LT} versus scattering coefficient μ_s with detection angle $\theta = 180°$, 135° and 121°. In this and subsequent figures, symbol = modeling results; lines = guides for the eye.

the scatterer radius r and the resultant anisotropy g, calculated from Mie theory [29]. The sphere concentration was varied such that the resultant μ_s was always 100 cm^{-1}. When scatterer radius r increases from ~0.1 to 0.48 μm, the anisotropy g rises quickly, from ~0.46 to 0.92. Further increases in scatterer size have smaller effects on g, as it remains high (0.81–0.95); a small relative minimum is seen at $r = 1.5\,\mu$m. The complex effects of g on depolarization are shown in Fig. 4(b). The top curve exhibits the variation in surviving linear N-resolved polarization fraction β_{LN} with $N = 1$ and $\theta = 180°$, for the anisotropy g range of 0.32–0.89. The surviving linear polarization fraction β_{LN} is relatively flat (~60%) when g is small (between 0.46 and 0.53). It is then seen to

undergo complex oscillations, with the highest value of ~81% and the lowest value of ~23% (note that the results in Figs. 2 and 3 correspond to this particular minimum). The surviving total linear polarization fraction β_{LN} for $\theta = 180°$, the bottom curve of Fig. 4(b), follows the similar trend but with smaller values than $\beta_{LN=1}$, as expected. Further, we found that even the same anisotropy g value, resulting from different scatterer sizes as indicated in Fig. 4(a), can yield different surviving polarization fractions, as shown in Fig. 4(c). Scatter radii $r = 0.37$, 1.14, and 2.05 μm yields the same $g = 0.89$ from the Mie calculation, but produce different surviving linear polarization fraction $\beta_{LN=1}$ values: 53%, 21.5%, and 25%, respectively. The implication is that the anisotropy effect on the linear surviving polarization fraction β_{LN} is, at least in part, also dependent on the scatterer size.

This phenomenon can be further investigated by examining the single-scattering phase function from the Mie scattering calculations. Figure 5(a) plots the phase function in backscattering direction ($\Delta\theta = 175° - 180°$) against anisotropy g, with corresponding scatterer size marked beside each data point. It demonstrates that the intensity of the scattering phase function in the backscattering direction varies significantly with anisotropy g, in a fashion similar to the depolarization trends observed in Fig. 4(b). It is, thus, not surprising that higher phase function intensity in the backscattering direction yields higher surviving linear polarization fractions detected at $\theta = 180°$. In analogy with Fig. 4(c), Fig. 5(b) plots the phase function intensity around the backscattering directions for the three scatterer sizes that yield the same g value of 0.89. Comparing the two figures, it is seen that backscattering phase function intensity variation and the surviving linear polarization fraction at $\theta = 180°$ detection direction show similar trends for these three scatterer sizes. It supports the above hypothesis that scatterer size affects the surviving linear polarization fraction [see Figs. 4(c) and 5(b)] through its effect on the phase function [see Figs. 4(b) and 5(a)]. Consequently, relying on a one-metric description of the phase function (its g value) is insufficient to understand the complexities of scattering-caused depolarization statistics.

The effect of sample birefringence on depolarization was also studied. Birefringence was added to the simulations by assigning the extraordinary refractive index change value close to the typical biological values ($n_e - n_o = 0.0001$), at a 45° angle in the x–y plane, as indicated in Fig. 1. Birefringence differentially retards polarization components that are parallel and perpendicular to the extraordinary axis. In transparent media, this leads to a transfer of light polarization states (linear ↔ elliptical ↔ circular ↔ elliptical ↔ linear, etc.); in turbid media, this effect is more complex due to multiple scattering [20]. Figure 6 displays the effect of the birefringence for the backscattering detection direction $\theta = 180°$ for incident linearly polarized light. Figure 6(a) shows

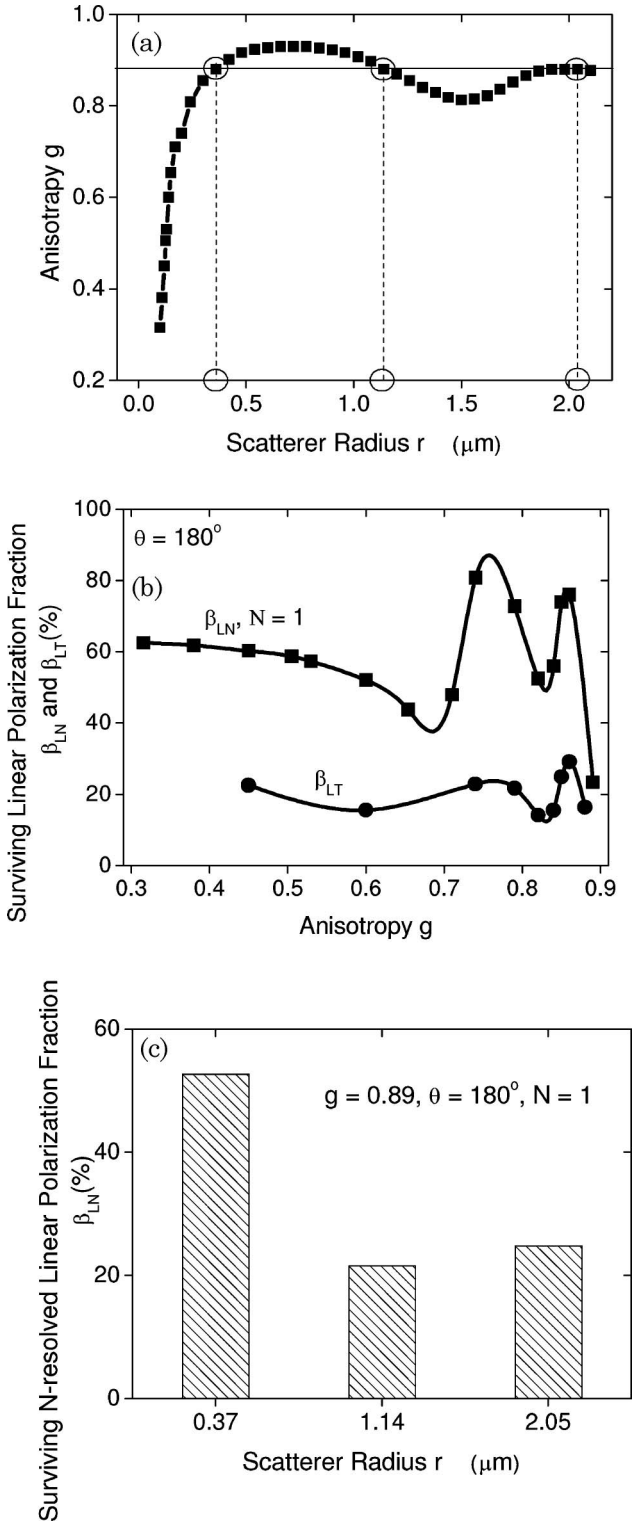

Fig. 4. Anisotropy g and scattering size r effects on depolarization of singly scattered light at detection angle $\theta = 180°$. (a) Anisotropy versus scatterer radius. (b) Surviving linear polarization fraction β_{LT} versus anisotropy g. (c) Surviving linear polarization fraction β_{LT} versus scatterer radius r for a g value of 0.89.

how the surviving linear polarization fraction β_{LN} changes with the number of scattering events N in the absence and presence of birefringence. Without

birefringence, β_{LN} drops linearly from ~23% to ~19% as the scattering-event number increases from 1 to 8. Conversely, with birefringence present, β_{LN} does not decrease with N but actually increases slightly to ~25% at $N = 8$. To explore this further, Fig. 6(b) shows that in the presence of birefringence, circular polarization states appear in the beam (from zero, as the incident light was linearly polarized) and increase; the surviving linear polarization fraction (the same dataset as in Fig. 6(a)] is also shown in the figure. This indicates that birefringence not only enhances linear polarization preservation, but transforms the linearly polarized light into elliptically polarized light. The increase of β_{LN} and β_{CN} with N implies that the birefringence effect is proportional to the photon path length. Larger N results in longer path length, thus the larger β_{LN} and β_{CN} values. This seems counterintuitive, but can be explained as follows. The longer path length increases the effect of birefringence, leading to more transfer from the input linear polarization to elliptical and circular polarizations; and these states have been shown to be better maintained in a high-g (forward-scattering) turbid media [2,30]. As the light undergoes additional scattering events and the path length further increases, the polarization transforms back from circular polarization to linear polarization, as the orthogonal polarization states being retarded return to their original relative phase (i.e., once again linearly polarized). However, as the circular polarization has been better maintained while propagating through the scattering media, the linear polarization fraction is now higher than that seen with

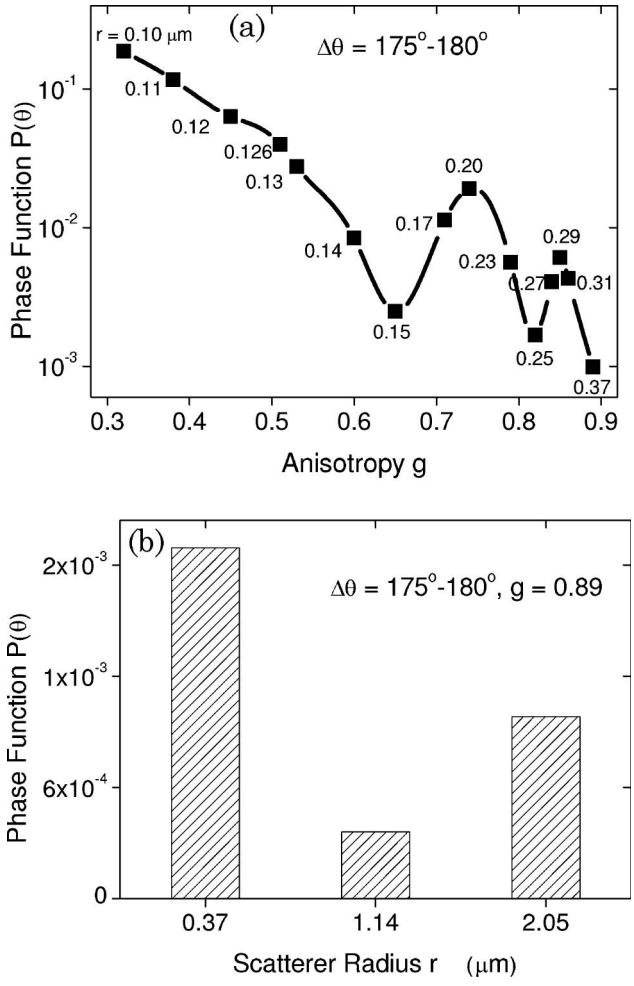

Fig. 5. Anisotropy g and scattering size r effects on phase function near backscattering direction ($\Delta\theta = 175°–180°$). (a) Phase function intensity near the backscattering direction versus anisotropy g. (b) Phase function intensity near the backscattering direction versus scatterer radius r.

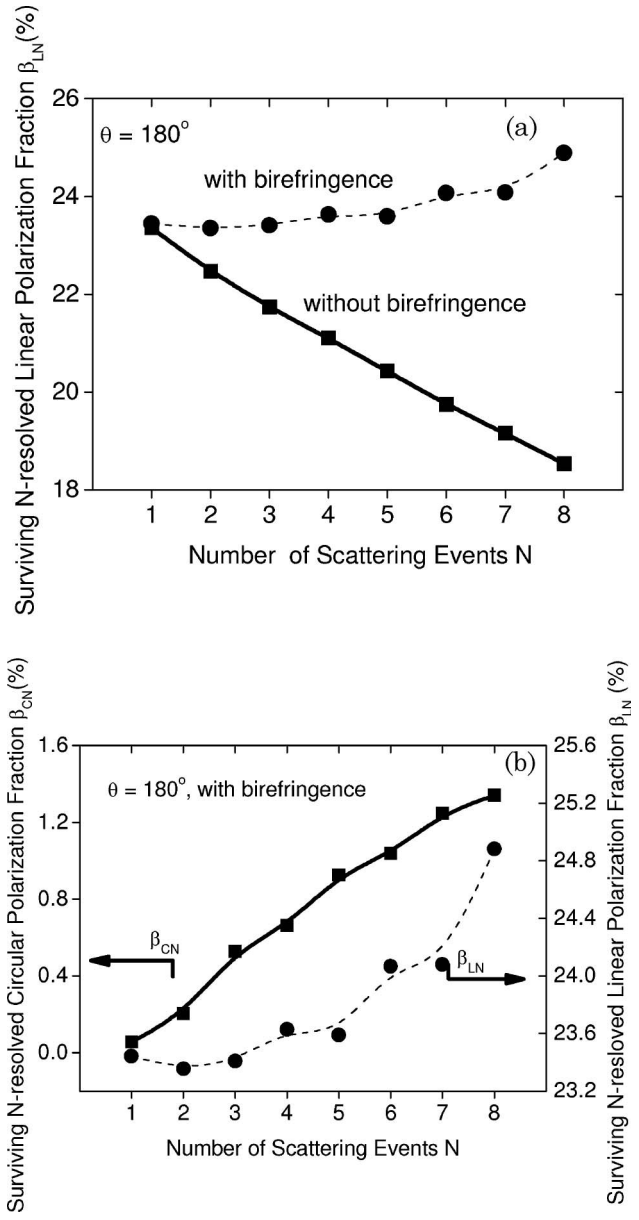

Fig. 6. Birefringence effects on depolarization. The detection angle θ is 180°. (a) Surviving linear polarization fraction β_{LN} versus the number of scattering events N (from 1 to 8) with and without birefringence; see text for Δn and **b** specification. (b) Surviving circular and linear polarization fractions β_{CN} and β_{LN} [the same dataset as in (a)] versus the number of scattering events N with birefringence.

no birefringence present. Importantly, it should be noted that the effects of birefringence are strongly dependent on the orientation of the extraordinary axis relative to the input beam and its linear polarization axis [20]; so the results in Fig. 6 are for a particular value of Δn and **b**.

C. Polarization State Effect on Depolarization

Our previous experimental studies have shown that circular polarization is better preserved in turbid media composed of forward-peaked scatterers [29], in accord with literature results [1,31]. To explore the details of this phenomenon, Fig. 7 shows MC simulation results for different incident polarization states (circular and linear), under otherwise identical conditions ($r = 2.05\,\mu$m, $g = 0.89$, $\mu_s = 100\,\text{cm}^{-1}$). Figure 7(a) plots the surviving circular and linear polarization fractions, β_{CN} and β_{LN}, against the number of scattering event N (from 1 to 79) at $\theta = 180°$. As expected [30], circular polarization is seen to be better preserved. After a single scattering event, circularly polarized incident light maintains ~45% of its polarization, while linearly polarized incident light only maintains ~24% of its polarization. Through ~50 scattering events, the linear polarization is nearly lost ($\beta_{LN=50} \sim 1.5\%$), whereas the incident circularly polarized light still maintains ~12% polarization. For the detection angle $\theta = 135°$ shown in Fig. 7(b), β_{CN} and β_{LN} both start off at ~60% for $N = 20$, the minimum number of scattering events needed for this detection geometry. With the increase in N, β_{CN} and β_{LN} begin to diverge. β_{LN} drops faster than β_{CN}, down to ~1% compared to 14% for β_{CN} at $N \sim 60$. Again, comparing Figs. 7(a) and 7(b) underscores the importance of the detection geometry—the trends seen for circular and linear polarization preservation are somewhat different (although $\beta_{CN} \geq \beta_{LN}$ for both detection angles), and a given number of scattering events N will result in different polarization preservation behavior depending on θ.

The total surviving circular polarization fractions β_{CT} and β_{LT} seen in Fig. 7(c) demonstrate that at all the detection angles in the backward hemisphere, circular polarization is better preserved than linear polarization. Further, the obtained degree of polarization $\text{DOP}_T = \beta_{CT} + \beta_{LT}$ from the simulations has similar values to β_{CT} when input is circularly polarized, and to β_{LT} when input is linearly polarized. It implies that the loss of circular and linear polarizations in the media is due to depolarization, not due to polarization state transformation (as seen from the discussions of Fig. 6, birefringence is the driving force for polarization state transformation). Figure 7 not only confirms the enhanced polarization preservation of the circularly polarized light input, but indicates that difference diminishes with the decrease of detection angle and the number of scattering events. In another words, the potential advantage of using circularly polarized light to probe turbid media seems most prominent in (singly) backscattering applications.

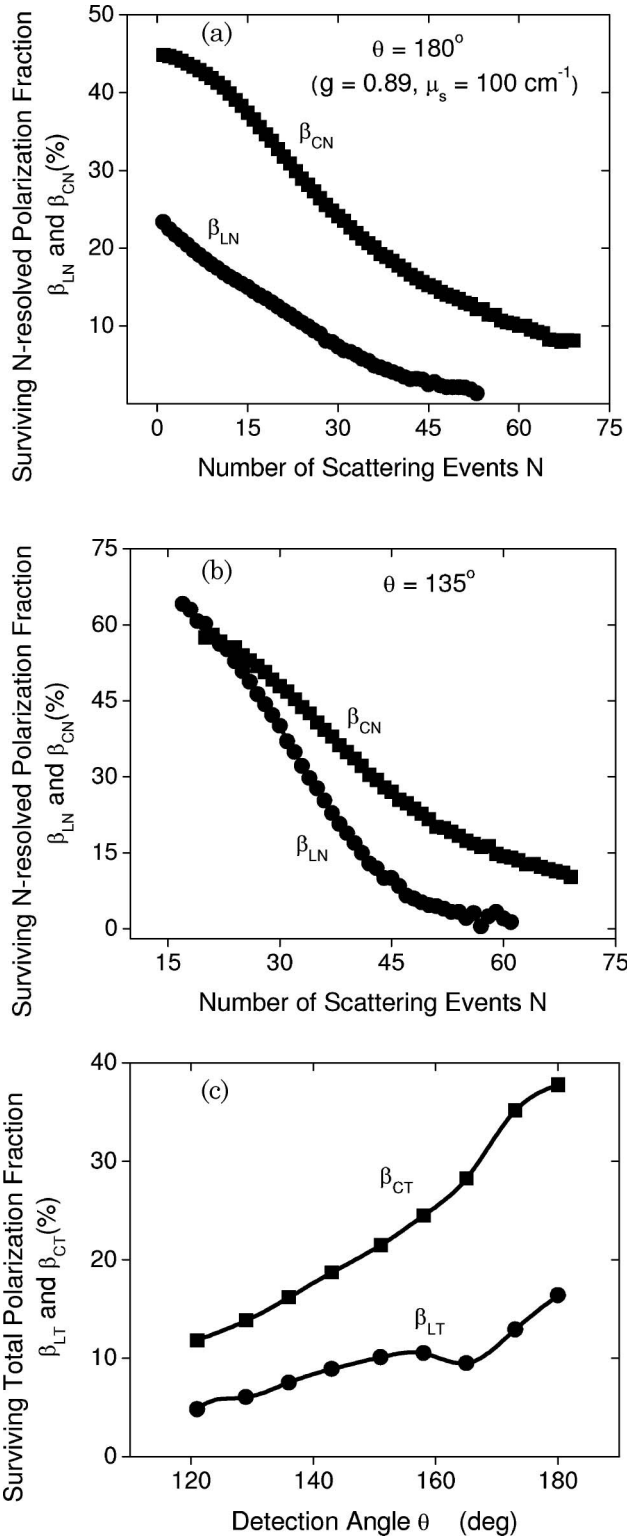

Fig. 7. Incident polarization state effect on depolarization. The anisotropy g and the scattering coefficient μ_s are fixed at 0.89 and 100 cm^{-1}, respectively. (a) Surviving linear and circular polarization fractions β_{LN} and β_{CN} versus the number of scattering events N at $\theta = 180°$. (b) Surviving linear and circular polarization fractions β_{LN} and β_{CN} versus the number of scattering events N at $\theta = 135°$. (c) Total surviving linear and circular polarization fractions β_{LT} and β_{CT} versus detection angle θ (99°–180°).

Finally, it is also interesting to note how the N-resolved β_N curves of Figs. 7(a) and 7(b) sum up to the β_T points seen in Fig. 7(c), when weighted by the number of photons I_N in each N bin. For example, the two β_{CN} curves in Figs. 7(a) and 7(b) ($\theta = 180°$ and $\theta = 135°$, respectively) span β_{CN} ranges of [45%–8%] and [68%–12%], respectively. Without the insights afforded by the current modeling study, one would then estimate that the total circular degree of polarization would be somewhat lower at $\theta = 180°$ compared to $\theta = 135°$. Yet this is not the case: when weighed by the values of I_N, there result $\beta_{CT}(180°) \sim 38\%$ and $\beta_{CT}(135°) \sim 16\%$ as seen in Fig. 7(c). This underscores the complexities of polarized light propagation in multiply scattering media and provides a useful example of the utility of developed formalism for studying the details of turbid media polarimetry.

4. Conclusions

We have studied light depolarization evolution in turbid media using polarization-sensitive Monte Carlo simulations. The photons exiting the cylindrical sample were tabulated based on the number of scattering events they encountered, and the surviving linear and circular polarization fractions of each photon group were studied for different detection geometries and optical properties of the turbid media. As expected, depolarization was seen to evolve at different rates when observed from different detection angles. Larger detection angles show a lower scattering number threshold for full depolarization (defined here as less than 1% of remaining incident polarization). For example, full depolarization requires ~50 scattering events at $\theta = 180°$, while it takes ~60 and ~70 scattering events for complete polarization randomization at $\theta = 135°$ and 99°, respectively. Besides scattering, depolarization is also affected by the polarization state of the incident light, and by the medium optical properties, such as scattering coefficient μ_s and anisotropy g (and even scatterer size r through its effect on the scattering phase function). In the presence of linear birefringence, evidence for polarization transformation (linear ↔ circular) was seen, which can actually lead to a slight *increase* in the polarization preservation with increasing number of scattering events. In summary, this study exhibits some of the subtleties of the light depolarization mechanisms in turbid media that involve a complex interplay of the effects of scattering number, detection geometry, anisotropy g, medium linear birefringence, and the polarization state of the incident light, and provides a methodology for their detailed investigations.

The authors thank the Natural Sciences and Engineering Research Council of Canada (NSERC) for financial support of this research.

Reference

1. D. A. Zimnyakov, Yu. P. Sinichkin, P. V. Zakharov, and D. N. Agafonov, "Residual polarization of non-coherently backscattered linearly polarized light: the influence of the anisotropy parameter of the scattering medium," Waves Random Media **11**, 395–412 (2001).
2. N. Ghosh, A. Pradhan, P. Kumar Gupta, S. Gupta, V. Jaiswal, and R. P. Singh, "Depolarization of light in a multiply scattering medium: effect of the refractive index of a scatterer," Phys. Rev. E **70**, 066607 (2004).
3. B. J. DeBoo, J. M. Sasian, and R. A. Chipman, "Depolarization of diffusely reflecting man-made objects," Appl. Opt. **44**, 5434–5445 (2005).
4. Y. Liu, Y. L. Kim, X. Li, and V. Backman, "Investigation of depth selectivity of polarization gating for tissue characterization," Opt. Express **13**, 601–611 (2005).
5. N. Ghosh, P. K. Gupta, A. Pradhan, and S. K. Majumder, "Anomalous behavior of depolarization of light in a turbid medium," Phys. Lett. A **354**, 236–242 (2006).
6. X. Guo, M. F. G. Wood, and I. A. Vitkin, "Monte Carlo study of pathlength distribution of polarized light in turbid media," Opt. Express **15**, 1348–1360 (2007).
7. I. Charalambous, R. Cucu, A. Dogariu, and A. Podoleanu, "Experimental investigation of circular light depolarization using polarization sensitive OCT," Proc. SPIE **6429**, 64291S (2007).
8. X. Guo, M. F. G. Wood, and I. A. Vitkin, "A Monte Carlo study of penetration depth and sampling volume of polarized light in turbid media," Opt. Commun. **281**, 380–387 (2008).
9. B. D. Cameron and H. Anumula, "Development of a real-time corneal birefringence compensated glucose sensing polarimeter," Diab. Technol. Ther. **8**, 156–164 (2006).
10. Yu. Lo and Tsung. Yu, "A polarimetric glucose sensor using a liquid-crystal polarization modulator driven by a sinusoidal signal," Opt. Commun. **259**, 40–48 (2006).
11. X. Guo, M. F. G. Wood, and I. A. Vitkin, "Stokes polarimetry in multiply scattering chiral media: effects of experimental geometry," Appl. Opt. **46**, 4491–4500 (2007).
12. E. Berrocal, D. L. Sedarsky, M. E. Paciaroni, I. V. Meglinski, and M. A. Linne, "Laser light scattering in turbid media Part II: Spatial and temporal analysis of individual scattering orders via Monte Carlo simulation," Opt. Express **17**, 13792–13809 (2009).
13. E. Berrocal, D. Y. Churmakov, V. P. Romanov, M. C. Jermy, and I. V. Meglinski, "Crossed source–detector geometry for a novel spray diagnostic: Monte Carlo simulation and analytical results," Appl. Opt. **44**, 2519–2529 (2005).
14. E. Berrocal, D. L. Sedarsky, M. E. Paciaroni, I. V. Meglinski, and M. A. Linne, "Laser light scattering in turbid media Part I: Experimental and simulated results for the spatial intensity distribution," Opt. Express **15**, 10649–10665 (2007).
15. D. Yu. Churmakov, V. L. Kuzmin, and I. V. Meglinski, "Application of the vector Monte-Carlo method in polarisation optical coherence tomography," Quantum Electron. **36**, 1009–1015 (2006).
16. I. V. Meglinski, V. P. Romanov, D. Y. Churmakov, E. Berrocal, M. C. Jermy, and D. A. Greenhalgh, "Low and high order light scattering in particulate media," Laser Phys. Lett. **1**, 387–390 (2004).
17. V. L. Kuz'min and I. V. Meglinski, "Backscattering of linearly and circularly polarized light in randomly inhomogeneous media," Opt. Spectrosc. **106**, 257–267 (2009).
18. D. Côté and I. A. Vitkin, "Balanced detection for low-noise precision polarimetric measurements of optically active, multiply scattering tissue phantoms," J. Biomed. Opt. **9**, 213–220 (2004).
19. D. Côté and I. A. Vitkin, "Robust concentration determination of optically active molecules in turbid media with validated three-dimensional polarization sensitive Monte Carlo calculations," Opt. Express **13**, 148–163 (2005).

20. M. F. G. Wood, X. Guo, and I. A. Vitkin, "Polarized light propagation in multiply scattering media exhibiting both linear birefringence and optical activity: Monte Carlo model and experimental methodology," J. Biomed. Opt. **12**, 014029 (2007).
21. B. Kaplan, G. Ledanois, and B. Drévillon, "Muller Matrix of dense polystyrene latex sphere suspensions: measurements and Monte Carlo simulation," Appl. Opt. **40**, 2769–2777 (2001).
22. F. Jaillon and H. Saint-Jalmes, "Description and time reduction of a Monte Carlo code to simulate propagation of polarized light through scattering media," Appl. Opt. **42**, 3290–3296 (2003).
23. C. F. Bohren and D. R. Huffman, *Absorption and Scattering of Light by Small Particles* (Wiley, 1983).
24. X. Guo, M. F. G. Wood, and I. A. Vitkin, "Angular measurements of light scattered by turbid chiral media using linear Stokes polarimeter," J. Biomed. Opt. **11**, 041105 (2006).
25. N. Ghosh, M. F. G. Wood, S. Li, R. D. Weisel, B. C. Wilson, R. Li, and I. A. Vitkin, "Mueller matrix decomposition for polarized light assessment of biological tissues," J. Biophotonics **2**,145–156 (2009).
26. S. Jiao, G. Yao, and L. V. Wang, "Depth-resolved two-dimensional Stokes vectors of backscattered light and Mueller matrices of biological tissue measured with optical coherence tomography," Appl. Opt. **39**, 6318–6324 (2000).
27. S. Lee, J. Kang, Ji. Yoo, M. Kang, J. Oh, and B. Kim, "Quantification of scattering changes using polarization sensitive optical coherence tomography," J. Biomed. Opt. **13**, 054032 (2008).
28. M. Sakami and A. Dogariu, "Polarized light-pulse transport through scattering media," J. Opt. Soc. Am. A **23**, 664–670 (2006).
29. K. C. Hadley and I. A. Vitkin, "Optical rotation and linear and circular depolarization rates in diffusively scattered light from chiral, racemic, and achiral turbid media," J. Biomed. Opt. **7**, 291–299 (2002).
30. X. Wang, G. Yao, and L. V. Wang, "Monte Carlo model and single-scattering approximation of the propagation of polarized light in turbid media containing glucose," Appl. Opt. **41**, 792–801 (2002).
31. A. Ishimaru, S. Jaruwatanadilok, and Y. Kuga, "Polarized pulse waves in random discrete scatterers," Appl. Opt. **40**, 5495–5520 (2001).